Materials and Solidification

Research Article

Phase equilibrium prediction for multicomponent alloys in phase field simulations using machine learning method

Yongjia Zhang[1], Peng Yu[2], Jianxin Zhou[2]✉, Yajun Yin[2], Xiaoyuan Ji[2], Xu Shen[2], Wen Li[2]

Cite this article: Zhang Y, Yu P, Zhou J, et al. *Materials and Solidification* 2025, **1**(2): 9580007. https://doi.org/10.26599/MAS.2025.9580007

ABSTRACT: The phase field (PF) model has been widely used for microstructure simulations during the solidification of multicomponent alloys. For multicomponent alloys, phase compositions need to be solved iteratively at every time step during phase field simulations because of the constraint of the phase equilibrium condition. The procedure requires frequent access to the thermodynamic database, which is time intensive. To accelerate the simulations, the machine learning method is used to predict the phase compositions. The machine learning method was implemented with graphics processing unit (GPU). The phase compositions of binary, ternary, and technical superalloys during solidification were predicted. A speedup ratio of 20.39 was obtained compared with the Newton iteration method for solving the phase compositions of the Al–Cu alloy. The prediction accuracy of the proposed method was evaluated. The machine learning method was subsequently applied to dendrite growth simulations via a phase field model. The dendrite tip radius versus growth velocity was examined via an analytical model, and good agreement was achieved. Finally, equiaxed dendrite growth was simulated, and the effect of the cooling rate was analyzed, which demonstrated the capacity of the proposed method.

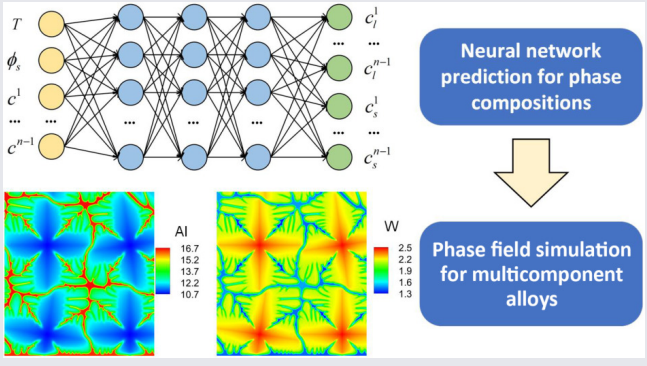

KEYWORDS: phase field method; machine learning; thermodynamic coupling; dendritic growth; GPU computing

1 Introduction

The phase field (PF) model has been widely applied to simulate dendritic growth during alloy solidification. The diffuse interface is employed in the PF model to track the phase interface, which makes it flexible to handle numerical treatment related to the interface region. The PF model has been adopted by many researchers to model dendritic growth during solidification for various alloys. However, for concentrated alloys, the linear phase diagram approximation may cause large deviations since the thermodynamics of each phase during the phase transformation are oversimplified. In addition, for multicomponent alloys, the widely used pseudobinary approximation in phase field simulations [1,2] also results in significant deviations. In the pseudobinary approximation, the lack of real thermodynamic parameters reduces the simulation accuracy for the composition and phase morphology. A binary surrogate alloy was used for the multicomponent CMSX-4 alloy, and only Al and Ti were used to estimate the thermodynamic parameters in the study of Isensee and Tourret [1]. Hence, the liquidus slope remains to be adjusted to match the real dendritic growth dynamics. By using the thermodynamic parameters for full multicomponent alloys via machine learning approaches, the evolution of different phases can be accurately predicted without additional adjustment [3]. By coupling with a thermodynamic database, PF simulations can reduce the aforementioned deviation and achieve high precision by considering accurate driving forces of phase transition and phase composition. Coupling with thermodynamics is important for phase transformation simulations of concentrated alloys and multicomponent alloys [4,5]. The effect of the Ni/Al content on the particle size distribution can be quantitively analyzed for Fe–Cu–Mn–Ni–Al alloys via full consideration of thermodynamic parameters [4]. Yang *et al.* [5] obtained the relationship between the dendrite arm spacing and solidification conditions by coupling the real thermodynamics of CMSX-4 alloy. The coupling method improved the simulation accuracy and was helpful for obtaining the power law variations for determining the dendrite arm spacing.

The multiphase field (MPF) model proposed by Steinbach *et al.* [6] can be easily coupled to a thermodynamic database and has been applied to the solidification simulation of a variety of alloys [5,7–9]. However, the MPF model coupled with a thermodynamic

[1] School of Energy and Mechanical Engineering, Jiangxi University of Science and Technology, Nanchang 330013, China. [2] State Key Laboratory of Materials Processing and Die & Mould Technology, Huazhong University of Science and Technology, Wuhan 430074, China.

✉ Corresponding author. E-mail: zhoujianxin@hust.edu.cn

Received: December 12, 2024; Revised: March 10, 2025; Accepted: March 26, 2025

database is time intensive since the phase compositions of coexisting phases should be iteratively solved with a quasiequilibrium constraint at all interface grids during every time step. The multiternary extrapolation method [10] and high-precision extrapolation [11] were proposed to obtain the phase compositions via thermodynamic extrapolation. These methods require sophisticated calculations to obtain quasiequilibrium data. The calculation process is usually performed via commercial thermodynamic software, which restricts its wide application for researchers. The improvement in the extrapolation accuracy of the phase composition is usually limited, although high extrapolation accuracy of the chemical driving force can be obtained by using a second-order scheme according to the results of Yang *et al.* [11]. To reduce the computational time, Fattebert *et al.* [12] proposed a solver for phase compositions via GPU, which can be easily integrated into the PF model coupling thermodynamic database.

Recently, the machine learning method has been applied to phase field simulations [13]. Nomoto *et al.* [3] adopted the neural network method to accelerate the nonequilibrium thermodynamics calculation. In their work, the chemical potential and the Gibbs energy molar density with a given temperature and phase composition were predicted via the neural network method, where a speedup ratio of five was obtained for the thermodynamic calculation procedure compared with direct access to the thermodynamic database. This work demonstrated the advantage of machine learning in reducing the calculation time, especially for multicomponent alloys. Jiang *et al.* [14] constructed a neural network method with one hidden layer of 150 nodes to predict the quasiequilibrium of a ternary alloy via the Kim–Kim–Suzuki (KKS) model [15]. Ren *et al.* [16] used a machine learning model with 4 hidden layers to predict the phase compositions during Al–Cu alloy solidification and applied it to simulations of equiaxed and columnar dendritic growth.

Overall, the existing machine-learning-aided prediction of phase compositions for multicomponent alloys has been applied to predict quasiequilibrium [14], but it has not been applied to phase field simulations of multicomponent alloys and technical alloys. Only the solidification of the Al-Cu binary alloys was simulated by the finite-interface dissipation model MPF model. The prediction accuracy and convergence lack sufficient analysis. In addition, previous studies focused on central processing unit (CPU)-based simulations. Currently, with the development of GPU hardware, GPU-based simulations have demonstrated high parallel performance, such as dendritic growth simulations via the PF model [17,18] and the cellular automaton model [19,20]. Therefore, in this work, we used a machine learning method to predict the phase compositions of multicomponent alloys. A neural network model with 3 hidden layers was designed to further improve the accuracy of the model for multicomponent alloys compared with that with one hidden layer [14]. The compositions of solute elements were used as outputs, which is different from the work of Nomoto *et al.* [14]. This made it more convenient to couple the phase field equation. The prediction accuracy for multicomponent alloys was improved. The model was implemented on GPU. The prediction accuracy of the phase compositions was analyzed, and dendritic growth simulations during solidification of the CMSX-4 alloy were simulated.

2 Numerical model

2.1 Multiphase field model

In the present study, the MPF model [21] was adopted to model the dendritic growth of multicomponent alloys. In the MPF model, each phase is defined by a phase field $\{\phi_\alpha(x,t)\}$, which represents the phase fraction of the α phase, and a composition field $\{c_\alpha(x,t)\}$ in the corresponding phase. The free energy function (F) can be deduced via the integration of the free energy density (f) (Eq. (1)):

$$F(\{\phi_\alpha\},\{c_\alpha\}) = \int_\Omega f(\{\phi_\alpha\},\{c_\alpha\}) \tag{1}$$

The free energy density (f) consists of the interface energy density and the chemical free energy density (Eq. (2)):

$$\begin{aligned} f &= f^{\text{intf}}(\{\phi_\alpha\}) + f^{\text{hem}}(\{\phi_\alpha\},\{c_\alpha\}) \\ &= \sum_{\alpha=1}^{\nu}\sum_{\beta=\alpha+1}^{\nu}\frac{4\sigma_{\alpha\beta}}{\nu\eta_{\alpha\beta}}\left(-\frac{\eta_{\alpha\beta}^2}{\pi^2}\nabla\phi_\alpha\nabla\phi_\beta+\phi_\alpha\phi_\beta\right)+\sum_{\alpha=1}^{\nu}\phi_\alpha f_\alpha(c_\alpha) \end{aligned} \tag{2}$$

where $\sigma_{\alpha\beta}$ is the interface energy between the α phase and the β phase. $\eta_{\alpha\beta}$ is the interface width. ν is the number of phases.

The temporal evolution of the phase fields is derived as Eq. (3):

$$\frac{\partial\phi_\alpha}{\partial t} = -\sum_{\beta\neq\alpha}^{\nu}M_{\alpha\beta}\left(\frac{\delta F}{\delta\phi_\alpha}-\frac{\delta F}{\delta\phi_\beta}\right) \tag{3}$$

where $M_{\alpha\beta}$ represents the interface mobility between the α phase and the β phase, and t represents the time. In the present study, only the liquid phase (l) and solid phase (s) are considered. Therefore, the deduced form of the phase field equation can be given as Eq. (4):

$$\begin{aligned} \frac{\partial\phi_s}{\partial t} = M_{sl}\Bigg[&\sigma_{sl}\left(\frac{1}{2}(\nabla^2\phi_s-\nabla^2\phi_l)+\frac{\pi^2}{2\eta_{sl}^2}(\phi_s-\phi_l)\right) \\ &+\frac{\pi}{\eta_{sl}}\frac{\sqrt{\phi_s\phi_l}}{v^m}\Delta G_{sl}\Bigg] \end{aligned} \tag{4}$$

where σ_{sl} is the anisotropic interface energy, v^m is the molar volume, and ΔG_{sl} is the thermodynamic driving force, which can be given by Eq. (5):

$$\Delta G_{sl} = g_l - g_s - \sum_{i=1}^{n-1}\tilde{\mu}^i(c_l^i - c_s^i) \tag{5}$$

where g_l and g_s are the molar Gibbs energies of the solid phase and liquid phase, respectively. The diffusion potential of the ith component $\tilde{\mu}^i$, can be determined by $\tilde{\mu}^i = \mu^i - \mu^n$ where μ^i and μ^n are the chemical potentials of the ith component and the solvent, respectively. c_l^i and c_s^i are the compositions of the ith components in the liquid phase and the solid phase, respectively. The phase compositions (c_l^i and c_s^i) should satisfy the equal diffusion potential condition (Eq. (6)):

$$\tilde{\mu}^i = \frac{\mathrm{d}g_l}{\mathrm{d}c_l^i} = \frac{\mathrm{d}g_s}{\mathrm{d}c_s^i} \tag{6}$$

Then, combined with the mass balance condition for each component (Eq. (7)):

$$\phi_s c_s^i + \phi_l c_l^i = c^i \tag{7}$$

For an n-component system, ($2n$–2) equations for the phase compositions (c_l^i and c_s^i) can be obtained. By using the Newton solver, the phase compositions can be obtained.

The solute diffusion equation with an anti-trapping current is given as Eq. (8):

$$\frac{\partial c^i}{\partial t} = \nabla\left[\sum_{\alpha=s,l}D_\alpha^i\phi_\alpha\nabla c_\alpha^i+\frac{\eta_{sl}}{\pi}(c_l^i-c_s^i)\sqrt{\phi_s\phi_l}\frac{\partial\phi_s}{\partial t}\frac{\nabla\phi_s}{|\nabla\phi_s|}\right] \tag{8}$$

where D_α^i is the diffusion coefficient of the ith component in the α phase. After solving Eqs. (6) and (7) at each grid during a time step, the obtained phase compositions (c_l^i and c_s^i) can be used to solve the solute diffusion equation.

The governing equations for the phase fields and composition fields in the MPF model were solved on uniform grids. The finite volume method with an explicit Euler scheme was employed. The computation was accelerated by the GPU-based parallel computing technique [22].

2.2 Machine learning model for phase composition prediction

The MPF model can be directly coupled with thermodynamic data via a thermodynamic database. The thermodynamic driving force (ΔG_{sl}) can be calculated from the thermodynamic data of each phase when the phase compositions (c_l^i and c_s^i) are obtained. For multicomponent alloys consisting of n components, we need to calculate the chemical potential of each component in each phase to deduce the diffusion potential of the ith component ($\tilde{\mu}^i$). For a multicomponent system, the molar Gibbs energy for a given phase α is as Eq. (9):

$$g_\alpha = \sum_{i=1}^{n} c_\alpha^i g_0^i + RT\sum_{i=1}^{n} c_\alpha^i \ln c_\alpha^i + g_\alpha^{ex} \tag{9}$$

where g_0^i is the Gibbs energy of the pure element i, the second part represents the ideal mixing contribution, R is the gas constant, and T is the temperature. The last term is the excess Gibbs energy, which can be expressed by the Redlich–Kister polynomial for binary systems and Redlich–Kister–Muggianu for ternary systems. Then, the chemical potential can be deduced by combining the derivatives of g_α^{ex} with respect to the composition [5]. The chemical potential of each component can be used to deduce the diffusion potentials ($\tilde{\mu}_l^i$ and $\tilde{\mu}_s^i$). Finally, the obtained $(2n-2)$ equations, noted as $\boldsymbol{L}$, about the phase compositions are expressed as Eq. (10):

$$\boldsymbol{L}(c_l, c_s) = \begin{cases} \tilde{\mu}_l^1 - \tilde{\mu}_s^1 = 0 \\ \phi_s c_s^1 + \phi_l c_l^1 - c^1 = 0 \\ \cdots \\ \tilde{\mu}_l^{n-1} - \tilde{\mu}_s^{n-1} = 0 \\ \phi_s c_s^{n-1} + \phi_l c_l^{n-1} - c^{n-1} = 0 \end{cases} \tag{10}$$

The composition of the solute element (c^1, c^{n-1}) is known for each grid. The phase fractions (ϕ_s and ϕ_l) are not independent since, for a two-phase system, they satisfy $\phi_s + \phi_l = 1$. For simplicity, we represent the composition set of solute elements as $c = [c^1, c^2, \ldots, c^n]$. Therefore, the set of local temperatures (T), the phase fractions (ϕ_s), and the solute compositions (c) can be considered as inputs, which can be denoted as $\{T, \phi_s, c\}$. The output can be represented as $\{c_l, c_s\}$, which are the compositions of each element in the liquid phase and solid phase.

Before the phase compositions are predicted, training data should first be generated. Hence, we briefly introduce the strategy of solving Eq. (10). To solve the nonlinear equations ($\boldsymbol{L}$), the Newton solver can be applied. The phase composition $\{c_l, c_s\}$ is represented as a solution vector (c_{ls}). By using a suitable initial value of c_{ls}, the solution vector (c_{ls}) can converge with iterations (Eq. (11)):

$$c_{ls}^{m+1} = c_{ls}^m - J^{-1} r(c_{ls}^m) \tag{11}$$

where J is the Jacobian of the nonlinear equations ($\boldsymbol{L}$), r is the residual of the equations ($\boldsymbol{L}$), and m is the number of iterations. Convergence can usually be reached with 5 iterations. Since the Jacobian (J) is the derivative of $\boldsymbol{L}$ with respect to each composition (c_l^i and c_s^i), we use the difference quotient to estimate the corresponding partial derivative. The Jacobian (J) satisfies the relationship ($J_{ij} = \partial r_i / \partial r_{ls}^j$) where r_i is the ith residual, and c_{ls}^j is the jth phase composition in composition set $\{c_l, c_s\}$. During the iterations, the inverse matrix (J^{-1}) is obtained via LU decomposition. In this work, the Newton solver was implemented in the C++ language, and the thermodynamic database was parsed via OpenCalphad [23].

A neural network model was constructed via the open source machine learning library PyTorch. The neural network model consists of an input layer, 3 hidden layers, and output layers, as shown in Fig. 1. The ReLU activation function and dropout regularization are used in the neural network model. For a multicomponent system with n components, the input layer has $(n+1)$ nodes, and the output layer has $(2n-2)$ nodes. The mean squared error (MSE) is defined as a mean squared formulation as Eq. (12):

$$\mathrm{MSE} = \frac{1}{M}\sum_{i=1}^{M}(y_i - y_i^*)^2 \tag{12}$$

where M is the dimension size of the data, y_i is the training data value, and y_i^* is the estimated value. The three hidden layers consist of 400, 100, and 50 layers. The Adagrad optimizer, which is an adaptive gradient algorithm, was used to train the neural network model. A learning rate of 0.01 was adopted in this study. Owing to the high computational performance of GPU, model training was performed on GPU.

3 Results and discussion

3.1 Phase composition prediction in Al–Cu binary alloy

The Al-Cu binary system with thermodynamic data [24] was first used as an example to generate the training data. In the training data, the composition of c^{Cu} around the Al-rich corner of the Al–Cu phase diagram was selected with the aim of simulating solidification of the Al-4.0 at% Cu alloy. In the training data, the temperature (T) ranges from 840 to 900 K since the liquidus temperature of Al–4.0 at%Cu is approximately 909 K. Ten thousand ($50 \times 10 \times 20$) data points for $\{T, \phi_s, c\}$ accompanied by the phase compositions $\{c_l, c_s\}$ obtained by the Newton solver are generated to train the neural network model. MSEs during training are shown in Fig. 2. With 39,232 iterations, the model training was completed with MSE error of 6×10^{-4}.

In a multicomponent system with n components, the relative error of the phase composition is defined as $(c_\alpha^{i,*} - c_\alpha^i)/c_\alpha^i$ for a given α phase of the ith component where c_α^i is the exact solution obtained via the Newton solver, and $c_\alpha^{i,*}$ is the predicted value.

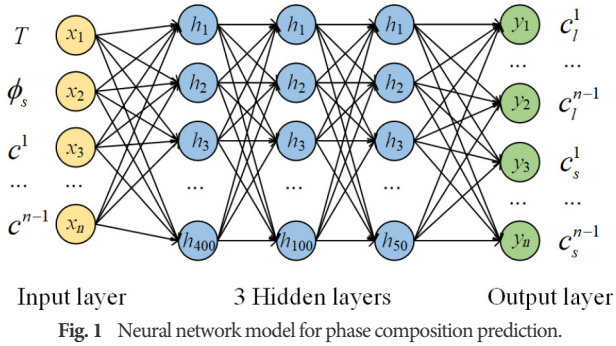

Fig. 1 Neural network model for phase composition prediction.

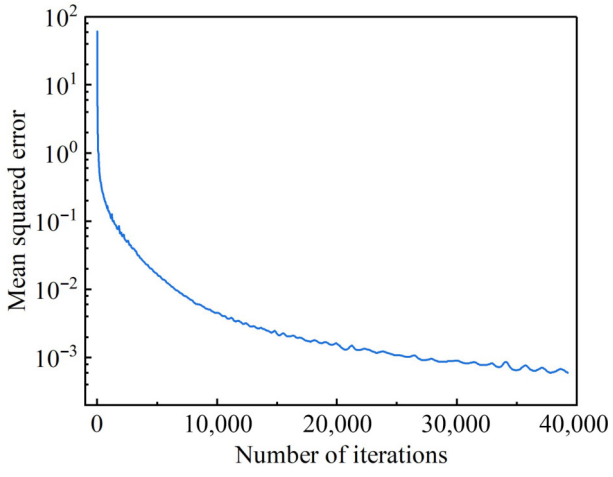

Fig. 2 Mean squared error during training of Al-Cu binary system.

The relative errors of the phase compositions (c_l^{Cu} and c_s^{Cu}) in the liquid phase and solid phase via prediction are given in Fig. 3.

The results indicated that the prediction error for 92% of the dataset is less than 1.0% for the composition of the liquid phase, as shown in Fig. 3(a). A test dataset with five thousand samples was used for error estimation, and the dataset was obtained via the Newton solver. Only a small percentage of the dataset has a large relatively large prediction error, which ranges from 4.0% to 7.0%. For the composition of the solid phase, the prediction error was greater than that of the liquid phase. This phenomenon may be caused by the small value of the partition coefficient of the Al–4.0 at% Cu alloys, which resulted in a small value of c_s^{Cu}. Owing to the intensive segregation between the solid and liquid phases of Cu, the value of c_s^{Cu} is approximately one tenth of the value of c_l^{Cu} obtained via the Newton solver. In fact, c_s^{Cu} and c_l^{Cu} are not independent because of the mass conversion relation ($\phi_s c_s^{Cu} + \phi_l c_l^{Cu} = c^{Cu}$). Therefore, we can calculate c_s^{Cu} via the predicted value of c_l^{Cu} instead of using the prediction value of c_s^{Cu} to avoid unexpected large prediction errors of c_s^{Cu}.

The distributions of data with large errors (3%–10%) and small errors (< 1%) were analyzed for the Al-Cu binary system. The error of the liquid phase composition was analyzed and is shown in Fig. 4. The corresponding error of the solid phase composition is given in Fig. 5. Among the data with large prediction errors for the liquid phase composition, the input Cu composition is small (less than 0.6 wt%). Most of the input (*C*) ranges from 0.2 wt% to 0.45 wt%, and its proportion is approximately 94%. Among the data with small errors, no significant difference was observed. The input C is uniformly distributed from 0 to 12 wt% as the input setting. According to the results of thermodynamic calculations, the partition coefficient for Al–4.0 at% Cu is small. Hence, the Cu concentration in the solid phase is low, which results in large errors in c_s^{Cu} in Fig. 3(b). In addition, as the input composition decreases, the phase compositions (c_s^{Cu} and c_l^{Cu}) decrease. Therefore, large prediction errors occurred when the input composition was less than 0.45% (Fig. 4(a)).

Among the data with large prediction errors for the solid phase composition, most of the input C ranges from 0 to 7 wt% among the data with large errors (3%–10%). Most of the input C ranges from 2 to 10 wt% among the data with small errors (< 1%). The results indicated that the prediction error of the liquid phase composition was sensitive to the input composition. An input

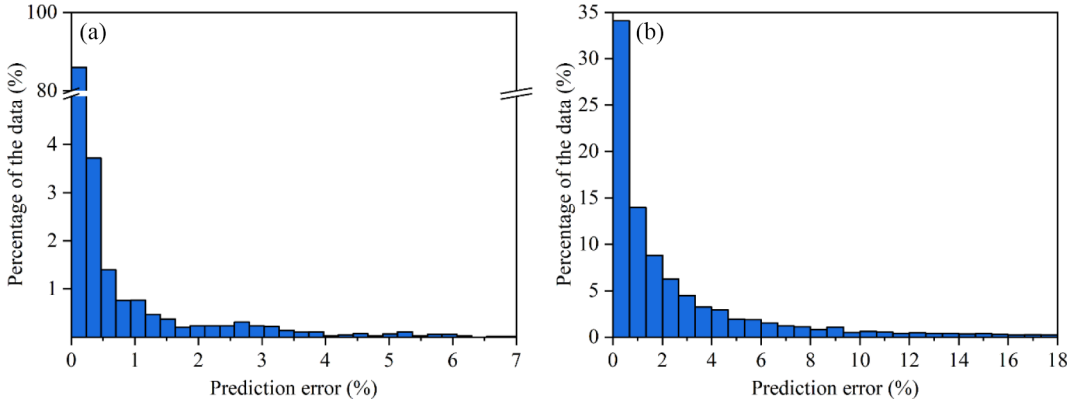

Fig. 3 Distribution of relative error of neural network predictions for Cu in (a) liquid phase and (b) solid phase.

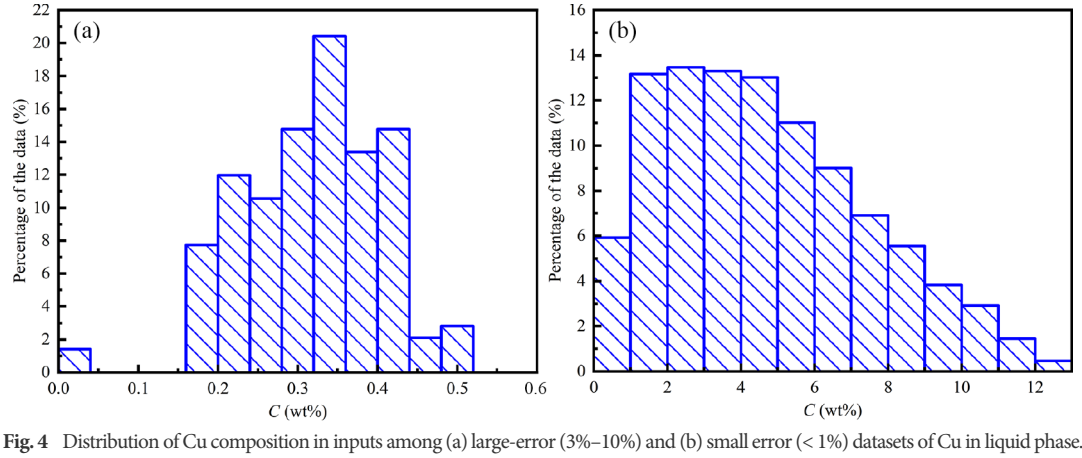

Fig. 4 Distribution of Cu composition in inputs among (a) large-error (3%–10%) and (b) small error (< 1%) datasets of Cu in liquid phase.

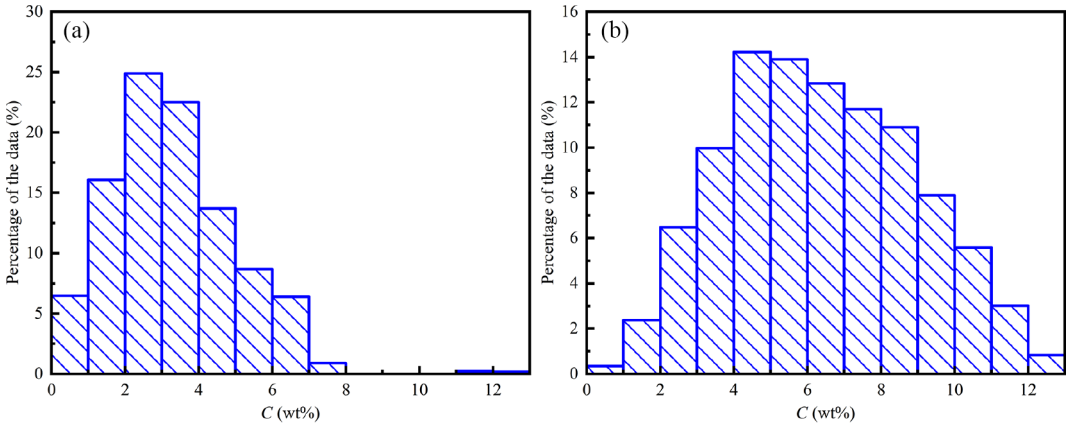

Fig. 5 Distribution of Cu composition in inputs among (a) large-error (3%–10%) and (b) small error (< 1%) datasets of Cu in solid phase.

composition close to zero leads to a large error. However, the prediction error of the solid-phase composition was not sensitive.

To compare the calculation times, the phase compositions were obtained via the Newton iteration method and the neural network model. The results of the Newton solver were obtained on CPU via a single thread. The results of the neural network model were obtained on the GPU. The calculations for the Newton solver were tested on an Intel Core i7-7700 (3.6 GHz). The neural network model was trained on an NVIDIA RTX 2070 GPU. The prediction model was then called via the LibTorch implemented in the C++ language because of its high computational performance compared with the prediction in the Python environment. On the other hand, using LibTorch in C++ will make coupling with GPU-based parallel computation convenient for the MPF model. The calculation times for phase compositions via the Newton solver and neural network prediction are given in Table 1.

For 10 thousand data points, the calculation time of the neural network prediction is 1.99×10^{-3} s, which is significantly less than that of the Newton solver. The speedup ratio is defined as the ratio of the calculation time of the Newton solver and the neural network prediction. As the amount of data increases from 10 thousand to 100 thousand data points, the speedup ratio of the neural network predictions reaches approximately 20. The training time in the present study is approximately 15 min for 100 thousand data points, whereas a training time of 112 min is needed in the work of Jiang *et al.* [14]. The shorter training time demonstrated the high computational performance of the present model on PyTorch. In this case, the time for neural network predictions is 1.82×10^{-2} s, which is only approximately 1/500 of the time using the model developed by Jiang *et al.* [14]. The results indicated that the neural network based on GPU is a time-saving algorithm compared with the model in Ref. [14]. The main source of the speedup comes from the hardware (peak performance of GPU vs CPU) according to our testing. A Newton solver was also implemented on GPU. The thermodynamic parameters were stored in code without using OpenCalphad. The performance of the GPU-based Newton solver was 8 times faster than that of the CPU-based Newton solver. The comparison was performed with the same hardware. In Ref. [12], a speedup of 277× was obtained by using V100 GPU. The difference in the speedup was caused mainly by the different peak performances of these GPUs.

For the solving time to generate the dataset, in our model, 3.71×10^{-1} s is needed when the Newton solver is used, whereas when the least squares method is used, 7 minutes is needed in Ref. [14]. Although in their work, 4 equations for phase

Table 1 Calculation time of Newton solver and neural network prediction

Amount of data (10^3)	10	50	100
Neural network training (s)	114.21	396.27	909.76
Newton solver (s)	3.72×10^{-2}	1.86×10^{-1}	3.71×10^{-1}
Neural network prediction on CPU (s)	1.65×10^{-2}	7.60×10^{-2}	1.53×10^{-1}
Neural network prediction on GPU (s)	1.99×10^{-3}	9.27×10^{-3}	1.82×10^{-2}
Speedup ratio	18.69	20.07	20.39

compositions were solved for a ternary alloy, the corresponding computational cost did not significantly increase compared with that of the binary system. The calculation time for a Ni–Al–Cr ternary system is given in the next section for further comparison. Compared with the Newton solver, the least squares method has better stability since the Newton solver may not converge if the initial solution vector is not selected properly. To overcome this drawback, the phase diagram was calculated via a thermodynamic database, and then the equilibrium partition coefficients at different temperatures were recorded to assist in the initialization of the phase compositions. During our testing, all the solution vectors converged over a wide range of input compositions and temperatures. With increasing input data, the prediction accuracy for c_l^{Cu} improved. The proportions of data with small errors (< 1%) for c_l^{Cu} were 92%, 96%, and 96% with 10k, 50k, and 100k input data, respectively. However, no significant improvement was observed for the prediction accuracy of c_s^{Cu}.

3.2 Phase composition prediction in Ni–Al–Cr ternary alloy

Ni–15Al–5Cr alloys (at%) were selected to verify the prediction accuracy of the ternary system. The solidification path was calculated via the thermodynamic data of Huang *et al.* [25]. The face-centered cubic (FCC) phase originated from the liquid phase. The variations in the phase fraction and phase composition with temperature are given in Fig. 6. The solidification range is 1671–1685 K. The partition coefficients of Al and Cr are approximately 0.88 and 0.89, respectively.

Then, the 20 thousand (20 × 10 × 10 × 10) data points for $\{T, \phi_s, c\}$ were generated as the inputs to train the neural network model. The temperature range of the inputs covered the whole solidification range of Ni–15Al–5Cr. Figure 7 shows the mean squared error with different learning rates (lr) during training. Learning rates of 0.002, 0.008, 0.01, 0.02, and 0.05 were used for training. MSE is reduced to 0.01 with a few iterations and then gradually converges to the required accuracy of 6×10^{-4}. The shortest training time of 187.41 s was obtained with a learning rate of 0.01. When the learning rate increased to 0.05, the MSE

frequently increased to a large value during training, as shown in Fig. 7. When the learning rate of 0.002 was adopted, the training time was the longest among these cases. As shown in Fig. 7, a learning rate near 0.01 is suitable for the training process.

The distributions of the relative errors of the neural network predictions for phase compositions are shown in Fig. 8. The test dataset with four thousand samples was used for error estimation.

In this case, the results indicated that the maximum relative error of the Al composition in each phase was less than 0.07%, and for Cr, the maximum was less than 0.15%. In Figs. 8(a) and 8(c), most of the relative errors of the Al composition were less than 0.02%. The Cr composition in each phase can be deduced from the corresponding Al composition according to the mass conservation relationship. Therefore, the obtained results demonstrated the high accuracy of the neural network model. Since the partition coefficient of Al and Cr in the Ni–Al–Cr system is close to 1.0, the segregation is not intensive for Al and Cr in the solid and liquid phases, which may lead to high prediction accuracy. The calculation time of the newton solver to generate 100 thousand data points was 9.93 s. It was reported that 112 min were needed when the least squares method was used [14]. Hence, the Newton solver has high efficiency for solving nonlinear equations with equal diffusion potential conditions. In addition, the prediction accuracy improved significantly compared with the work of Jiang *et al.* [14], where the maximum value of prediction

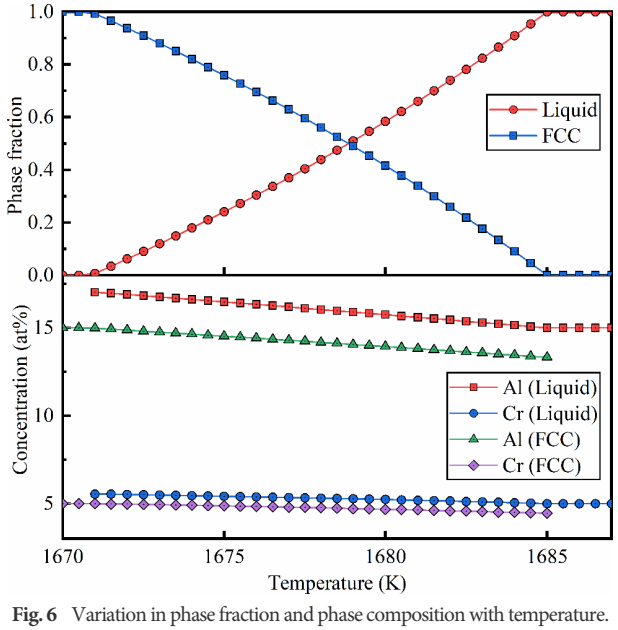

Fig. 6 Variation in phase fraction and phase composition with temperature.

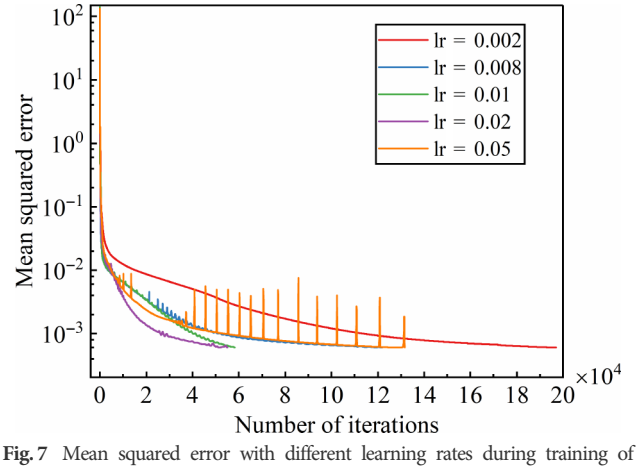

Fig. 7 Mean squared error with different learning rates during training of Ni–Al–Cr ternary system.

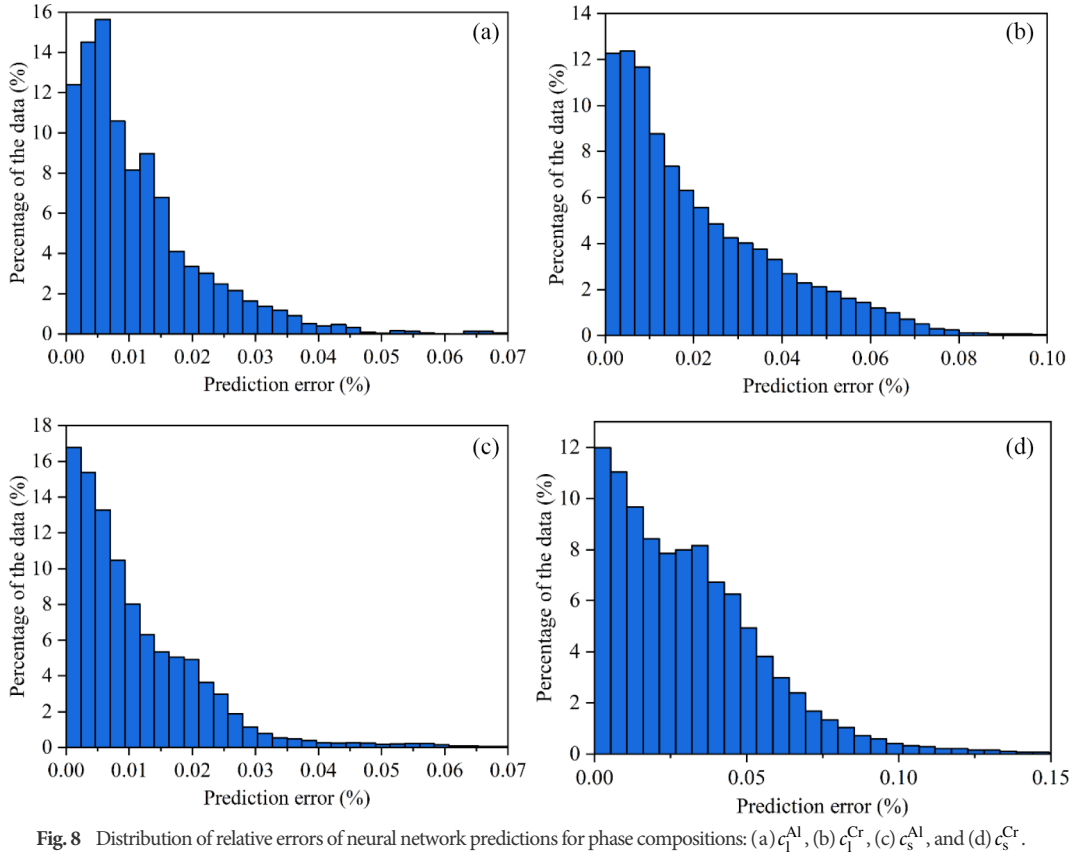

Fig. 8 Distribution of relative errors of neural network predictions for phase compositions: (a) c_l^{Al}, (b) c_l^{Cr}, (c) c_s^{Al}, and (d) c_s^{Cr}.

error reached 6% for the Al-Cu-Mg ternary system. The maximum values of prediction error for Al and Cr were 0.07% and 0.15%, respectively, in the present study. Instead of using one hidden layer, 3 hidden layers were adopted in the present work. This may contribute to the improvement in accuracy. To further improve the prediction accuracy, a dataset of 2000 thousand ($20 \times 10 \times 100 \times 100$) inputs for $\{T, \varphi_s, c\}$ was tested. The maximum error remains at approximately 0.07% for Al and 0.09% for Cr in the liquid phase. The proportion of small error data (< 0.02%) increased slightly. This increase was related to the small interval of the input compositions of Al and Cr. Training time of 4.6 h was used to achieve convergence. Compared with the Newton solver, it is more difficult to improve the prediction accuracy by increasing the amount of input data. When the Newton solver is used, the convergence can be obtained by three or four iterations to an accuracy of 1×10^{-6} and can further improve to 1×10^{-9} via several iterations. Hence, considering the accuracy, the Newton solver method is better for simulations with high accuracy. The advantage of neural network prediction is that the time consumed is related only to the training process. Once the model is trained, the prediction procedure does not require more time, even if the accuracy is improved when a large dataset is used.

3.3 Phase composition prediction for CMSX-4 superalloy

The CMSX-4 nickel-based superalloy was selected to predict the phase composition. The alloy composition used for the thermodynamic calculation was Ni–12.72Al–9.9Co–7.48Cr–0.95Re–2.18Ta–1.28Ti–2.11W (in at%), as simplified by Yang *et al.* [26]. Minor Mo and Hf were not considered in the present calculation since the influence of these two elements on the primary FCC phase can be ignored. The range of the solidification temperature is 1656–1573 K. A total of 10 thousand data points were used for phase composition prediction for the eight-component system. The cumulative distribution function (CDF) of the prediction error was statistically analyzed, and CDF was defined as $F(a) = \int_0^a f(x^\varepsilon)\,\mathrm{d}x^\varepsilon$, where $f(x^\varepsilon)$ is the probability density function of the prediction error (x^ε). The CDF of the prediction error for the phase composition is given in Fig. 9.

The results indicated that high prediction accuracy was obtained for the prediction of the liquid phase composition for most elements, except for the Re element, as shown in Fig. 9(a). For most elements, the value of CDF, $F(0.3\%)$, is greater than 99% for the prediction error of the liquid phase compositions. For the prediction error of the solid phase composition shown in Fig. 9(b), the value of CDF, $F(0.2\%)$, is greater than 99.7% for Al, Co, Cr, and W. The maximum prediction error for the Re element was 1.04% in the solid phase. The maximum prediction errors for Ta and Ti are close to 10.0%, which is significantly greater than those of the other elements. The partition coefficients of Re, Ta, and Ti are reportedly 1.59, 0.68, and 0.85 [27], respectively, which indicates relatively strong segregation between the solid and liquid phases. As observed in the case of the Al-Cu binary system, a strong intensity of segregation will cause a relatively high prediction error. Therefore, this phenomenon also occurred in the prediction of the CMSX-4 alloy. Similarly, the element with low accuracy in a given phase can be obtained via the mass conservation relation according to the corresponding composition in the other phase. The present calculation was a simplification of the CMSX-4 composition. The minor elements Mo and Hf affect the real solidification path, which also affects the quasiequilibrium solution stability. One restriction of the present method is the limitation of the thermodynamic database. Although the open source software OpenCalphad was employed to provide convenient access to thermodynamic calculations, the prediction is dependent on an open thermodynamic database. The prediction accuracy remains restricted by the database. When the alloy compositions are out of range of the open database, the commercial database and its interface module should be used to provide the data for the training process. Another shortcoming is the requirement of training data. The present study considered only two phases during solidification. For multiphase systems, such as eutectic or peritectic reactions, the stability of the Newton solver depends on a suitable initial guess of the solution. A possible approach to improve the solving stability is to consider the equilibrium condition and the extrapolated approximation [11].

3.4 Dendrite growth during solidification of CMSX-4 superalloy

The proposed prediction method is applied to dendrite growth during solidification of the CMSX-4 superalloy. To verify this method, dendrite growth during directional solidification was analyzed. The dendrite tip radius versus velocity was examined via the Kurz-Giovanola-Trivedi (KGT) analytical model. The KGT model was extended to multicomponent alloys for examination of the CMSX-4 alloy according to Isensee *et al.* [1]. The simulations were performed in a two-dimensional rectangular domain. A constant temperature gradient of 4.4 K/mm is applied in the computational domain. The initial undercooling at the bottom is

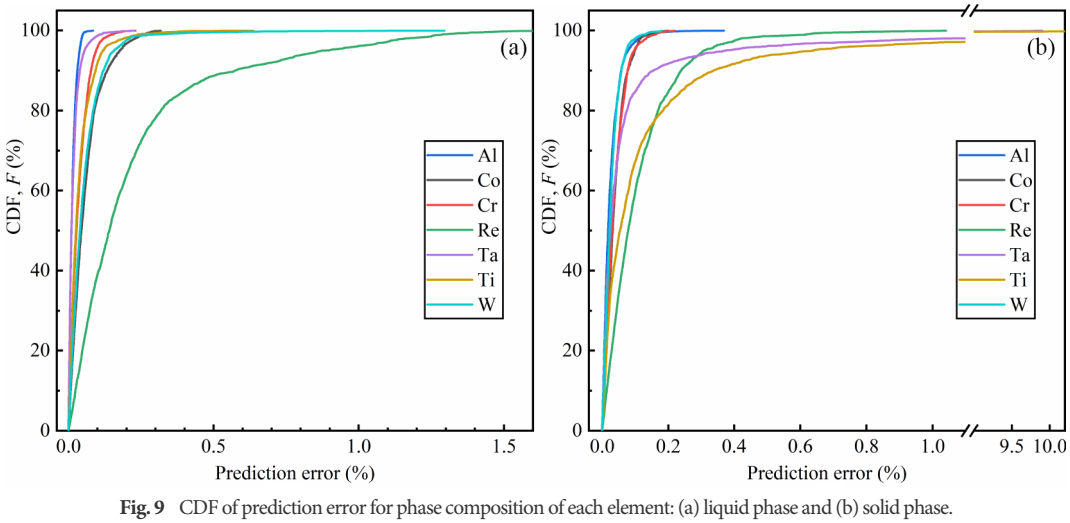

Fig. 9 CDF of prediction error for phase composition of each element: (a) liquid phase and (b) solid phase.

10 K. The pulling velocities are set as 2, 5, 10, 20, 50, and 100 μm/s for comparison with the KGT model. According to the KGT model, the tip radius decreases with increasing velocity. The mesh size was selected according to the radius to ensure accuracy, and the relationship between the mesh size and tip radius satisfied $\Delta x < R_{tip}/8$, where Δx is the mesh size, and R_{tip} is the tip radius. The simulations ended after a long growth distance. The kinetic anisotropy coefficient is 0.05, and the static anisotropy coefficient is 0.02 [5]. The molar volume is 7.8×10^{-6} m^3/mol. The interface energy is 0.161 J/m^2. The interface width ($\eta_{\alpha\beta}$) was determined according to the relation ($\eta_{\alpha\beta} = 4\Delta x$). Figure 10 shows the tip radius versus velocity obtained via the KGT model and phase field simulations. The dendrite tip was fitted via a parabolic polynomial to calculate the tip radius. The inset in Fig. 10 shows the fitting curve of the dendrite tip with a pulling velocity of 20 μm/s. The simulation results indicated that the tip radius decreased from 19.53 to 3.92 μm when the pulling velocity increased from 2 to 100 μm/s. The simulation results agreed well with those of the LGK model, which demonstrated the capacity of the proposed prediction method.

Equiaxed dendrite growth was simulated, and the effect of the cooling rate on the solidification process was investigated. The computational domain is 2048 μm × 2048 μm. A uniform undercooling of 10 K is applied at the initial time. The cooling rates for the three simulations are 1, 5, and 10 K/s. The simulations ended when the total undercooling reached 60 K. The mesh size was 1 μm. Initially, 49 seeds with predefined orientations and locations were set, and the setting of seeds was the same for these three simulations. The simulation results are shown in Fig. 11. The results revealed that the Al concentration increased with a cooling rate of 10 K/s when the solid fraction reached 0.8. The results in Fig. 11(a) indicated that Al was enriched in the interdendritic region, and the maximum concentration reached 16.0 at%. As the cooling rate increased from 1 to 10 K/s, more side branches formed, as shown in Figs. 11(b)–11(d). The solid fraction of the simulation domain is given in Fig. 11(e). During solidification, the increase in the solid fraction was fast at the initial solidification stage and then slowed. The increasing peaks of the solid fraction occurred at 1642, 1632, and 1624 K for the cases with cooling rates of 1, 5, and 10 K/s, respectively. The element concentrations and the solid phase with a cooling rate of 10 K/s are shown in Fig. 12. A high degree of element segregation was observed. The Al, Ta, and Ti elements are enriched in the interdendritic region, and the Co, Cr, Re, and W elements are enriched in the dendrite core. The simulation results indicated that dendrites grow with cubic anisotropy, and several side branches can be observed. In the case of 10 K/s, approximately 2% of the time was spent in the neural network solver. For the whole PFM simulation, approximately 28% of the time was reduced. This significantly reduced the total calculation time. The present method can be used to investigate the microstructure evolution of nickel-base superalloys during initial solidification, which contributes to the design of commercial alloys.

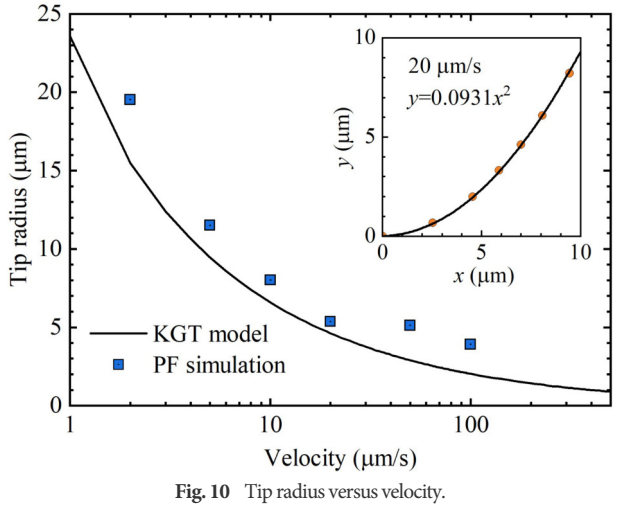

Fig. 10 Tip radius versus velocity.

4 Conclusions

The machine learning method was used for the prediction of phase equilibrium for multicomponent alloys. The proposed method was applied to dendrite growth simulations during solidification via the MPF model. The proposed machine learning method was faster than the Newton iteration solver for phase compositions, and a speedup ratio of 20.39 was obtained for the Al-Cu alloy utilizing GPU. The prediction accuracies of the Al-Cu binary alloy, Ni-Al-Cr ternary alloy, and CMSX-4 superalloy were examined. The degree of element segregation affects the prediction accuracy, and the prediction results of the phase

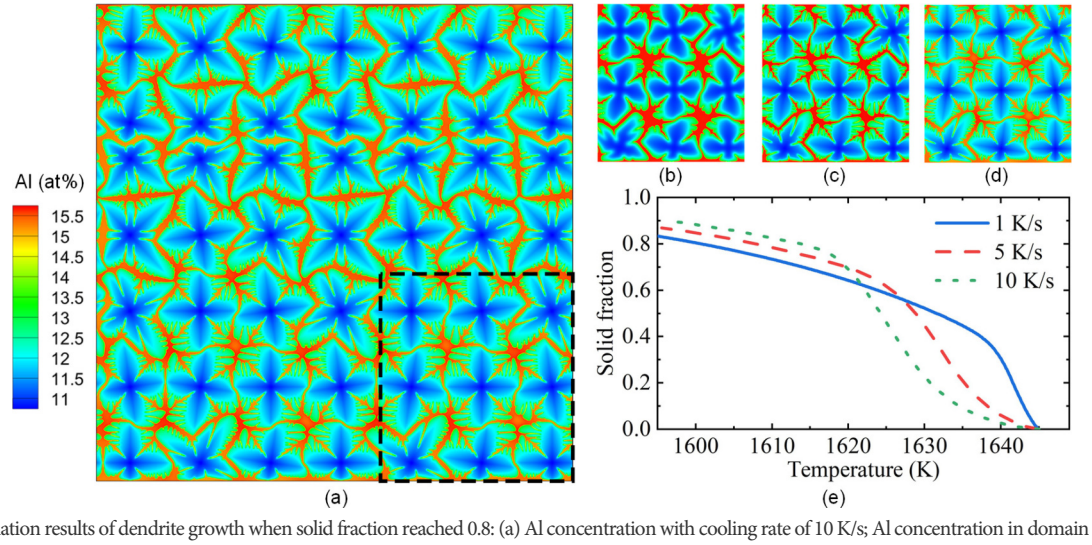

Fig. 11 Simulation results of dendrite growth when solid fraction reached 0.8: (a) Al concentration with cooling rate of 10 K/s; Al concentration in domain labeled with a dashed line with cooling rate of (b) 1 K/s, (c) 5 K/s, (d) 10 K/s, and (e) solid fraction versus temperature in the simulation domain.

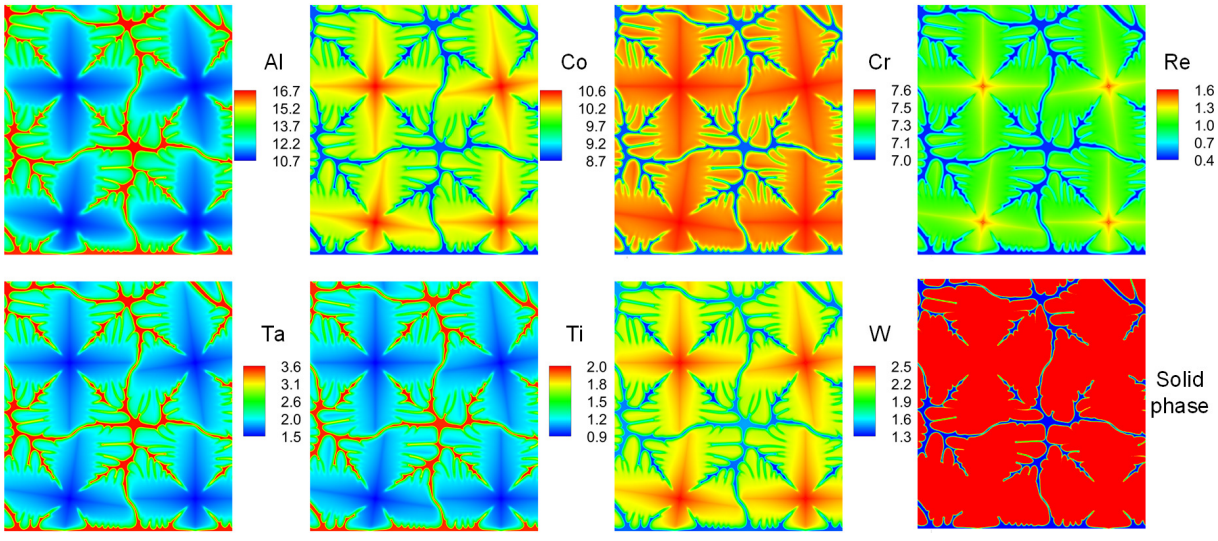

Fig. 12 Element concentrations and solid phase after complete solidification at cooling rate of 10 K/s.

compositions can be corrected via the mass conservation relation. The machine learning method is suitable for different alloys with multicomponent and two-phase systems. The present study indicated that the accuracy for different alloys varied significantly. For elements with large partition coefficients, the prediction accuracy was affected by the input composition. The improvement in accuracy achieved by increasing the number of datasets is limited. The relationship between the dendrite tip radius and the growth velocity obtained via the MPF simulations agreed well with that of the LGK model. Element segregation and dendrite branching during solidification were observed via simulations. The simulation results demonstrated the capacity of the proposed method. The application is limited to the thermodynamic database since only an open database is allowed with OpenCalphad software. The further improvement is the solving stability in the generation of input datasets. For accuracy improvement, the construction of suitable input datasets covering a wide range of compositions without excessive increases in the amount of data is a possible approach.

Acknowledgements

This work was funded by the Open Project of Jiangxi Provincial Key Laboratory of Additive Manufacturing for Implanted Medical Devices (No. 2024ZCZZSZ02), the High-level Talent Research Launch Project of JXUST (No. jxust-40) and the National Natural Science Foundation of China (No. 52201042).

Availability of data and materials

The data that support the findings of this study are available from the corresponding author upon reasonable request.

Competing interests

The authors have no competing interests to declare that are relevant to the content of this article.

References

[1] Isensee T, Tourret D. Convective effects on columnar dendritic solidification–A multiscale dendritic needle network study. *Acta Mater* 2022, **234**: 118035.

[2] Sun W, Yan R, Zhang Y, *et al.* GPU-accelerated three-dimensional large-scale simulation of dendrite growth for Ti_6Al_4V alloy based on multi-component phase-field model. *Comput Mater Sci* 2019, **160**: 149–158.

[3] Nomoto S, Wakameda H, Segawa M, Yamanaka A, Koyama T. Solidification analysis by non-equilibrium phase field model using thermodynamics data estimated by machine learning. *Model Simul Mater Sci Eng* 2019, **27**: 84008.

[4] Sun YY, Zhao YH, Zhao BJ, *et al.* Multi-component phase-field simulation of microstructural evolution and elemental distribution in Fe–Cu–Mn–Ni–Al alloy. *Calphad* 2020, **69**: 101759.

[5] Yang C, Xu QY, Liu BC. Primary dendrite spacing selection during directional solidification of multicomponent nickel-based superalloy: Multiphase-field study. *J Mater Sci* 2018, **53**: 9755–9770.

[6] Steinbach I, Pezzolla F, Nestler B, *et al.* A phase field concept for multiphase systems. *Phys D Nonlinear Phenom* 1996, **94**: 135–147.

[7] Tiaden J, Nestler B, Diepers HJ, *et al.* The multiphase-field model with an integrated concept for modelling solute diffusion. *Phys D Nonlinear Phenom* 1998, **115**: 73–86.

[8] Grafe U, Böttger B, Tiaden J, *et al.* Coupling of multicomponent thermodynamic databases to a phase field model: Application to solidification and solid state transformations of superalloys. *Scripta Mater* 2000, **42**: 1179–1186.

[9] Tegeler M, Shchyglo O, Kamachali RD, *et al.* Parallel multiphase field simulations with OpenPhase. *Comput Phys Commun* 2017, **215**: 173–187.

[10] Böttger B, Eiken J, Apel M. Multi-ternary extrapolation scheme for efficient coupling of thermodynamic data to a multi-phase-field model. *Comput Mater Sci* 2015, **108**: 283–292.

[11] Yang C, Xu QY, Liu BC. A high precision extrapolation method in multiphase-field model for simulating dendrite growth. *J Cryst Growth* 2018, **490**: 25–34.

[12] Fattebert JL, de Witt S, Perron A, *et al.* Thermo4PFM: Facilitating Phase-field simulations of alloys with thermodynamic driving forces. *Comput Phys Commun* 2023, **288**: 108739.

[13] Peivaste I, Siboni NH, Alahyarizadeh G, *et al.* Machine-learning-based surrogate modeling of microstructure evolution using phase-field. *Comput Mater Sci* 2022, **214**: 111750.

[14] Jiang X, Zhang RJ, Zhang C, *et al.* Fast prediction of the quasi phase equilibrium in phase field model for multicomponent alloys based on machine learning method. *Calphad* 2019, **66**: 101644.

[15] Kim SG, Kim WT, Suzuki T. Phase-field model for binary alloys. *Phys Rev E Stat Phys Plasmas Fluids Relat Interdiscip Topics* 1999, **60**: 7186–7197.

[16] Ren LY, Geng SN, Jiang P, *et al.* Numerical simulation of dendritic growth during solidification process using multiphase-field model aided with machine learning method. *Calphad* 2022, **78**: 102450.

[17] Sakane S, Aoki T, Takaki T. Parallel GPU-accelerated adaptive mesh refinement on two-dimensional phase-field lattice Boltzmann simulation of dendrite growth. *Comput Mater Sci* 2022, **211**: 111507.

[18] Sakane S, Takaki T, Ohno M, *et al.* Acceleration of phase-field lattice Boltzmann simulation of dendrite growth with thermosolutal convection by the multi-GPUs parallel computation with multiple mesh and time step method. *Model Simul Mater Sci Eng* 2019, **27**: 054004.

[19] Sabau AS, Yuan L, Fattebert JL, *et al.* An OpenMP GPU-offload implementation of a non-equilibrium solidification cellular automata model for additive manufacturing. *Comput Phys Commun* 2023, **284**: 108605.

[20] Zhang YJ, Zhou JX, Yin YJ, *et al.* Multi-GPU implementation of a cellular automaton model for dendritic growth of binary alloy. *J Mater Res Technol* 2021, **14**: 1862–1872.

[21] Eiken J, Böttger B, Steinbach I. Multiphase-field approach for multicomponent alloys with extrapolation scheme for numerical application. *Phys Rev E Stat Nonlin Soft Matter Phys* 2006, **73**: 066122.

[22] Zhang YJ, Zhou JX, Yin YJ, *et al.* Study on the solutal convection during dendrite growth of superalloy under directional solidification condition. *J Mater Res Technol* 2023, **23**: 3916–3927.

[23] Sundman B, Kattner UR, Palumbo M, *et al.* OpenCalphad—A free thermodynamic software. *Integr Mater Manuf Innov* 2015, **4**: 1–15.

[24] Buhler T, Fries SG, Spencer PJ, *et al.* A thermodynamic assessment of the Al–Cu–Mg ternary system. *J Phase Equilib* 1998, **19**: 317–333.

[25] Huang W, Chang YA. Thermodynamic properties of the Ni–Al–Cr system. *Intermetallics* 1999, **7**: 863–874.

[26] Yang C, Xu QY, Liu BC. Study of dendrite growth with natural convection in superalloy directional solidification via a multiphase-field-lattice Boltzmann model. *Comput Mater Sci* 2019, **158**: 130–139.

[27] Ganesan M, Dye D, Lee PD. A technique for characterizing microsegregation in multicomponent alloys and its application to single-crystal superalloy castings. *Metall Mater Trans A* 2005, **36**: 2191–2204.